Efficient and stable proton acceleration by irradiating a two-layer target with a linearly polarized laser pulse

H. Y. Wang, X. Q. Yan, J. E. Chen, X. T. He, W. J. Ma et al.

Citation: Phys. Plasmas **20**, 013101 (2013); doi: 10.1063/1.4773198
View online: http://dx.doi.org/10.1063/1.4773198
View Table of Contents: http://pop.aip.org/resource/1/PHPAEN/v20/i1
Published by the AIP Publishing LLC.

Efficient and stable proton acceleration by irradiating a two-layer target with a linearly polarized laser pulse

H. Y. Wang,[1] X. Q. Yan,[1,a)] J. E. Chen,[1] X. T. He,[1] W. J. Ma,[2,b)] J. H. Bin,[2] J. Schreiber,[2] T. Tajima,[2] and D. Habs[2]
[1]*State Key Laboratory of Nuclear Physics and Technology, Peking University, Beijing 100871, China and Key Lab of High Energy Density Physics Simulation, CAPT, Peking University, Beijing 100871, China*
[2]*Fakultät für Physik, Ludwig-Maximilians-Universität München, Am Coulombwall 1, 85748 Garching, Germany and Max-Planck-Institut für Quantenoptik, Hans-Kopfermann-Str. 1, 85748 Garching, Germany*

(Received 9 August 2012; accepted 7 December 2012; published online 3 January 2013)

We report an efficient and stable scheme to generate ~200 MeV proton bunch by irradiating a two-layer targets (near-critical density layer+solid density layer with heavy ions and protons) with a linearly polarized Gaussian pulse at intensity of 6.0×10^{20} W/cm^2. Due to self-focusing of laser and directly accelerated electrons in the near-critical density layer, the proton energy is enhanced by a factor of 3 compared to single-layer solid targets. The energy spread of proton is also remarkably reduced. Such scheme is attractive for applications relevant to tumor therapy. © *2013 American Institute of Physics*. [http://dx.doi.org/10.1063/1.4773198]

Energetic ion bunches produced by the interaction of ultraintense, ultrashort laser pulses with matter have attracted considerable attention due to their potential applications,[1] including injector for traditional ion accelerators, proton imaging and oncology, medical therapy, and inertial confinement fusion. An important goal, developing sources of laser-driven protons for radiation therapy of deep-seated tumors, requires 200 MeV proton beams with a small energy spread.[2]

Most of the experimental and theoretical studies on laser-driven ion acceleration are based on solid density targets. Two major acceleration mechanisms have been identified in this density regime: target normal sheath acceleration (TNSA)[3] and radiation pressure acceleration (RPA).[4] In TNSA, hot electrons are generated by the laser at the front surface and transported to the rear side of the target, establishing a sheath electrostatic field there. The sheath field, of order 10^{12} V/m, can accelerate the ions on the target back surface to MeV level. Proton beams with energies >60 MeV have been produced within TNSA regime, yet with large energy spreads.[5] In RPA, the radiation pressure at the front surface can boost the ion and electron layers synchronously as if they constitute a quasi-neutral plasma slab, where equilibrium between the electrostatic and the radiation pressures holds. It is favorable to suppress generation of hot electrons and the rapid decomposition of targets with circularly polarized laser pulses.[6] Recently Yin *et al.*,[7] Zhuo *et al.*,[8] and Qiao *et al.*[9] found that quasimonoenergetic ion beams can also be realized by using linearly polarized (LP) pulses. In order to produce mono-energetic ion beams in these regimes, extremely high laser intensity, sharp rising front, and ultrahigh laser contrast are mandatory and the quality of proton beam is sensitive to the target parameters.[4,8–10]

Recently, attentions have also been paid to near-critical targets for ion acceleration. Such targets are considered to have higher laser-plasma coupling efficiency.[11,12] Energetic ions are accelerated at the rear surface in this density regime by magnetic vortex formation[13] or the sheath field with its extended lifetime.[14] A three-layer target configuration was proposed by Sgattoni *et al.*[15] and Nakamura *et al.*[16] It was found that the presence of the near-critical plasma strongly increases the conversion efficiency and leads to enhanced acceleration for protons. In the mechanisms above, ion beams are not bunched and mono-energetic ion spectra have not been reported yet.

In this paper, we present a novel proton acceleration and bunching mechanism by combining a critical density layer (CDL) with a solid density layer (SDL) as targets. Differ from Refs. 15 and 16, here we consider a laser pulse with slightly higher intensity and larger spot size. Such laser pulse first experiences relativistic self-focusing process in CDL.[17] The self-focusing length increases with the initial laser spot size, which is in the order of tens of μm in case of a laser spot size diameter of about 10 μm. When the length of CDL is equal to the laser self-focusing length, the CDL acts as a plasma lens to generate higher intensity laser with steep rising front.[18] Meanwhile, energetic electrons are efficiently accelerated by the direct laser acceleration (DLA)[19,20] mechanism in the self-focused channel. When both shaped laser pulse and energetic DLA electrons arrive at the SDL, a stronger and longer-living stable sheath field is built at the rear surface as compared to a single-layer solid target, leading to more efficient proton acceleration and bunching. It is shown from simulations that a ~200 MeV proton bunch with energy spread of 12% can be generated at intensity of 6×10^{20}W/cm^2. Both the peak energy and the energy spread are significantly improved in comparison to the single-layer solid target (67 MeV with energy spread 57%). It should be noticed that neither a sharp rising temporal profile nor a super-Gaussian spatial profile (as flat top) of laser pulses is applied in these simulations. The optimum condition for the front CDL is presented. The acceleration processes and bunching mechanism are analyzed in detail.

a)x.yan@pku.edu.cn
b)Wenjun.Ma@physik.uni-muenchen.de

The simulations are performed with 2D PIC code KLAP2D.[22] The simulation space (120 μm $\times$ 40 μm) is composed of 9600 $\times$ 1600 cells along z and y directions. A linearly p-polarized laser pulse with a Gaussian envelope $a = a_0 \exp[-(y-y_0)^2/r_0^2]\exp[-(t-t_0)^2/\tau^2]$ in both the longitudinal (z) and the transverse (y) directions is normally irradiated from the left side ($z = 0\,\mu$m). We shall set $a_0 = 21$, corresponding to a peak laser intensity of 6.0×10^{20} Wcm^{-2} with laser wavelength $\lambda = 1\,\mu$m, $t_0 = \tau = 15T$, $r_0 = 6\,\mu$m, and $y_0 = 20\,\mu$m, where $T = 3.3$ fs is the laser period, corresponding to about 0.9 PW laser power and 50 J laser energy. A CDL plasma consisting of electrons and carbon ions is located between $10\,\mu\text{m} \le z \le 35\,\mu$m with an electron density $n_{e10} = 1.2n_c$, where the critical plasma density $n_c = m_e\omega^2/4\pi e^2$, m_e, e, and ω are electron mass, charge, and laser angular frequency, respectively. The SDL, attached behind the CDL, consists of a proton-carbon mixed plasma with thickness $d = 0.15\,\mu$m and electron density $n_{e20} = 60n_c$. The ratio of C^{6+}:H = 10:1. The number of particles per cell for each species is 200 for solid density layer and 36 for critical density layer. An initial electron temperature of 1 keV is used to resolve the initial Debye length, and ions are initially cold.

When the laser propagates through the CDL, it forms a self-focused channel containing most of the laser energy as shown in Fig. 1(a). The radius of the focused laser spot size can be estimated as $r_f = \frac{1}{\pi}\sqrt{\frac{a_0 n_c}{\sqrt{2}n_{e1}}}$,[18] where a_0 is the initial normalized laser intensity and n_{e1} is the initial near-critical electron density. For our simulation parameters, this gives a value of 1.125 μm, consistent with the simulation result (1.1 μm). The focused laser intensity is determined by the initial laser intensity, initial laser spot size, and plasma density, which should satisfy $a_f \le a_0\sqrt{r_0/r_f}$ for 2D case and $a_f \le a_0 r_0/r_f$ for 3D case, where a_0, r_f, and r_0 are the initial laser intensity, focused laser spot size, and initial laser spot size, respectively. In our simulation, the focused laser intensity $a_f \sim 1.8a_0 \le a_0\sqrt{r_0/r_f} = 2.3a_0$, as shown in Fig. 1(a). Together with the efficient laser shaping process, the laser pulse quickly deposits its energy in the CDL (mainly to the electrons). The trajectory and final energy gain of the electrons are strongly dependent on their initial position. Only those electrons propagating in the laser direction can be transported through the SDL and play a role in the ion acceleration process. Two typical groups of electrons are identified from simulation as shown in Figs. 1(b) and 1(c) (snow plow (SP) electrons in the green box and DLA electrons in the black box). The SP electrons, piling up at the front of the laser pulse due to the snow plow mechanism,[21] have density much higher than the background electron density. However, this group of electrons does not gain much energy from the laser pulse (see Fig. 1(d)). The second group of electrons experiences DLA via betatron resonance first found by Pukhov *et al.*[20] Under interaction of laser field and self-generated quasi-static electric and magnetic fields in the channel, these electrons oscillate at the betatron frequency

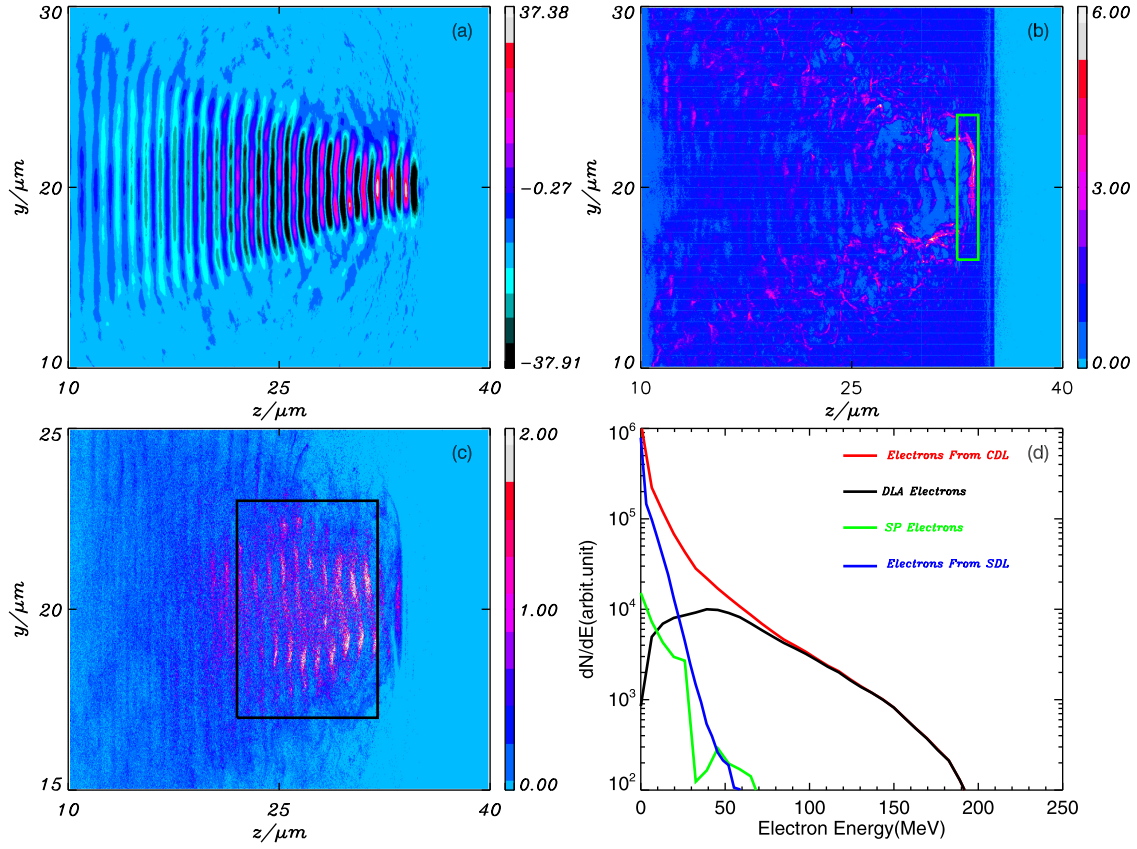

FIG. 1. Laser shaping process and efficient electron acceleration in CDL. (a) Laser envelope E_y (in units of $m_e c\omega/e$) at $t = 46T$, (b) normalized electron density n_{e1} in CDL at $t = 44T$, (c) the energy flux density of the electrons $E_f = \sum(\gamma - 1)m_e c^2 v_{ez}$ in CDL at $t = 44T$, and (d) the electron energy spectrum for all the electrons from CDL, DLA electrons, SP electrons at $t = 44T$ and electrons from SDL at $t = 60T$, the time is chosen when the electron cut-off energy reach maximum.

$\omega_\beta \approx \omega_p/(2\gamma)^{1/2}$ while comoving along the channel with the light. Here, γ is the relativistic factor and $\omega_p = 4\pi e^2 n_e/m_e$ is the plasma frequency. When ω_β coincides with the laser frequency, the channel resonance results in effective energy exchange between the laser field and the electrons. This betatron resonance behavior is clearly visible in Fig. 1(c), which shows the energy flux density of the electrons $E_f = \sum(\gamma - 1)m_e c^2 v_{ez}$. We see that the efficient DLA acceleration occurs when the laser propagates through the channel. The electrons oscillate longitudinally twice per laser period, leading to two electron bunches above and below the axis per laser wavelength. Fig. 1(d) shows the electron energy spectrum for all electrons from CDL, DLA electrons (electrons in black box as shown in Fig. 1(c)), SP electrons (electrons in green box as shown in Fig. 1(b)) at $t = 44T$, and electrons from SDL at $t = 60T$. It is found that the laser coupling efficiency is much higher in CDL than in SDL, which leads to both higher electron temperature and electron number. The laser conversion efficiency to all electrons in CDL, DLA electrons, SP electrons, and electrons in SDL is 26%, 11%, 0.8%, and 1.8%, respectively.

The details of acceleration process of the two-layer target (right column) and the single-layer solid target (left column) are shown in Figs. 2 and 3. Here, we set the SDL a two ion species (carbons and protons) with a low proton/carbon ratio, which is known to improve the proton energy spread.[3,23] In both single-layer and two-layer targets, the forward moving protons at rear side of the targets are quickly accelerated ahead of the carbons due to its higher charge to mass ratio, as shown in Figs. 2(a) and 2(b). For the two-layer target, in order to clearly show the contributions from different layers, the electron density from CDL (n_{e1}) and SDL (n_{e2}) is distinguished in Figs. 2(b) and 2(d), and we can see that electrons from CDL dominate in the proton acceleration process. Compared to the single-layer solid target, a stronger and longer sheath field is built at the rear side of the two-layer target, due to the combination of the shaped laser pulse and the energetic DLA electrons. This leads to more efficient proton acceleration and higher proton energy. For the two-layer target, a proton bunch with peak energy of about 150 MeV and energy spread of 14% is formed at $t = 75T$, which is about three times higher than the single-layer solid target (50 MeV with energy spread of 15% at $t = 65T$), as shown in Figs. 3(c) and 3(d).

Simulations with longer time are carried out in order to clarify the evolution of the proton bunch. For the single-layer solid target, at $t = 90T$ as the hot electrons quickly expand away, the protons are expanding in the longitudinal direction due to Coulomb explosion. A typical dual-peaked field structure is seen, as shown in Fig. 2(c). In this stage, the peak proton energy keeps almost the same, while the proton energy spread increases drastically (see Figs. 3(a) and 3(c)). An interesting observation is that for the two-layer target, the Coulomb explosion is significantly suppressed during the whole acceleration process. We attribute this result to two reasons: First, the proton density for the two-layer target is smaller due to more efficient and longer acceleration in the early stage (see Figs. 2(c) and 2(d)), thus its Coulomb explosion field is not so pronounced as the single-layer solid target; second, the sheath field for the two-layer target is stronger than that of the

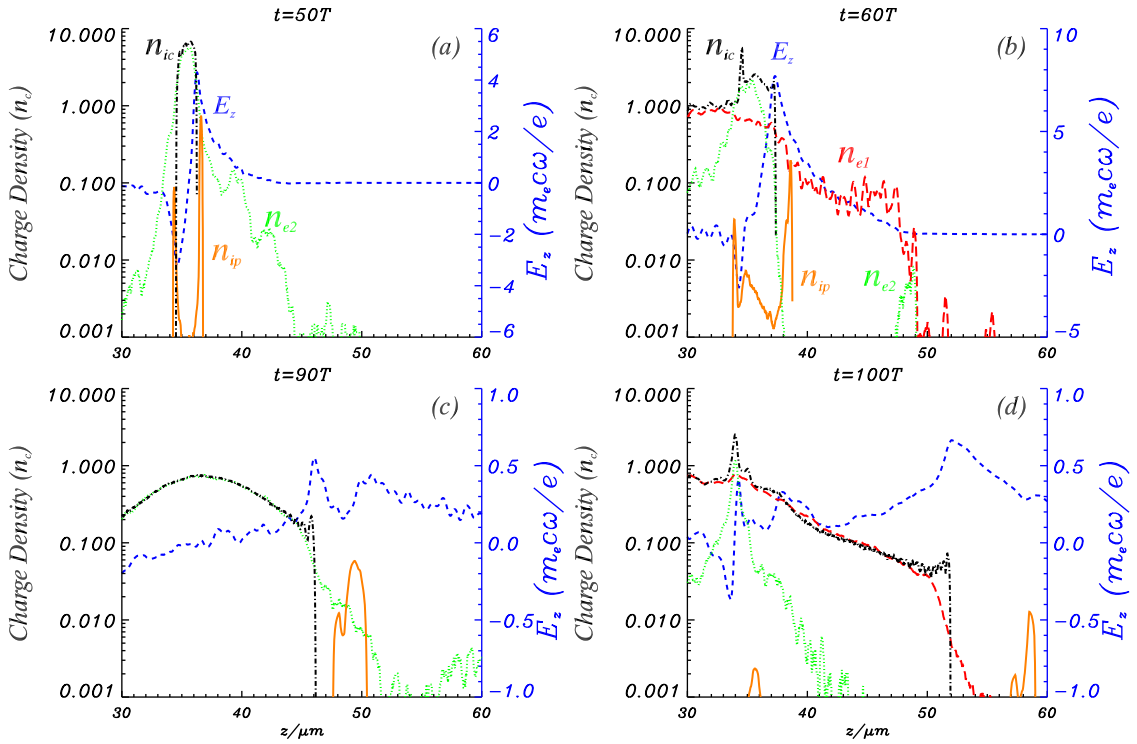

FIG. 2. The details of acceleration process of the two-layer target (right column) and the single-layer solid target (left column). (a) and (c) On axis longitudinal profiles of electron density n_{e2} (green dotted line), proton density n_{ip} (yellow solid line), carbon density $Z * n_{ic}$ (dark dashed-dotted line), and sheath field E_z (blue dashed line) for the single-layer solid target at $t = 50T$ and $t = 90T$, (b) and (d) On axis longitudinal profiles of CDL electron density n_{e1} (red long dashed line), SDL electron density n_{e2} (green dotted line), proton density n_{ip} (yellow solid line), carbon density $Z * n_{ic}$ (dark dashed dotted line), and sheath field E_z (blue dashed line) for the two-layer target at $t = 60T$ and $t = 100T$.

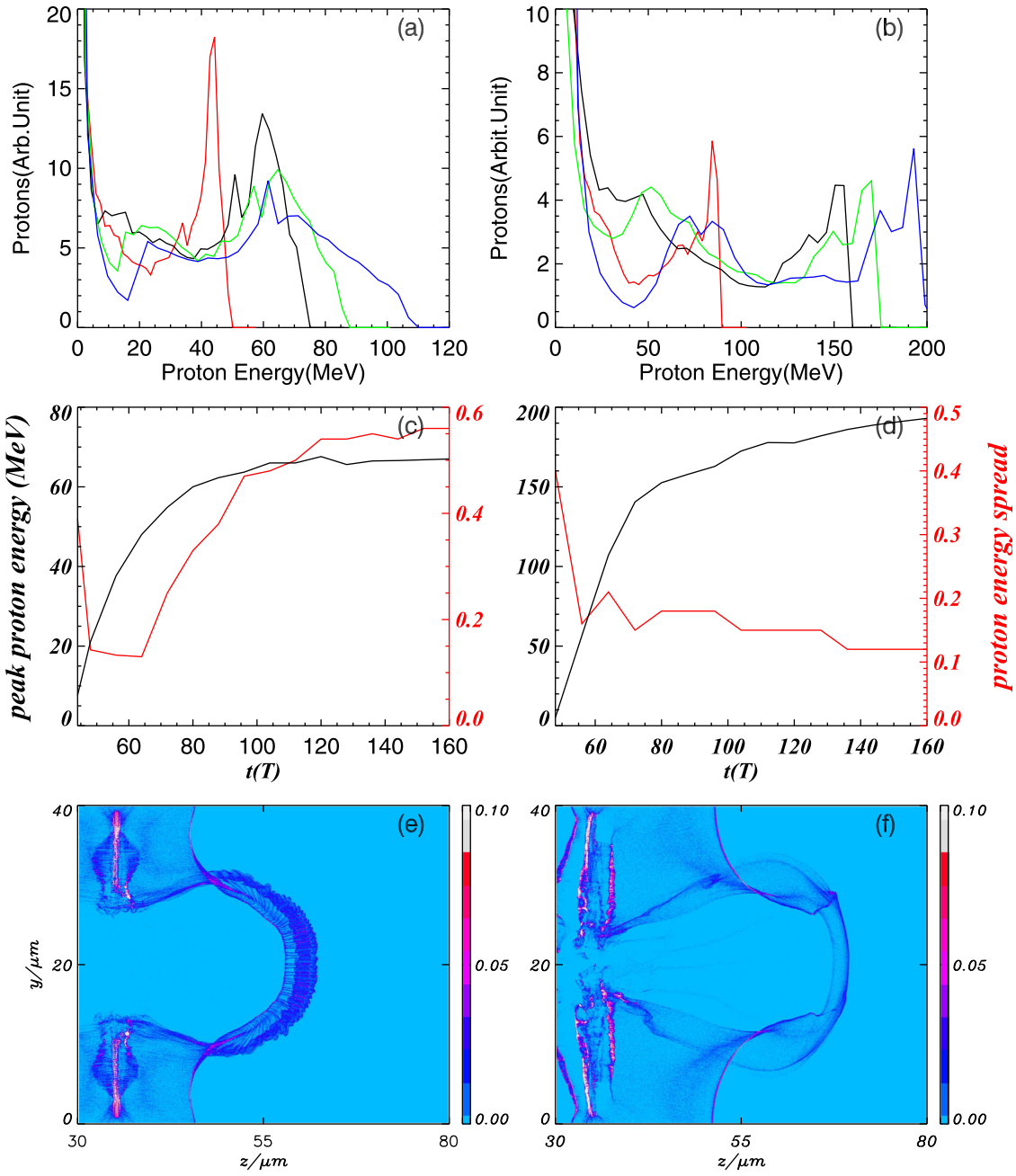

FIG. 3. Proton energy spectra at $t = 60$ (red), 80 (black), 100 (green), and $160\,T$ (blue) for (a) single-layer solid target, (b) two-layer target; time evolution of the peak proton energy and proton energy spread for (c) single-layer solid target, (d) two-layer target; proton density at $t = 120\,T$ for (e) single-layer solid target, (f) two-layer target.

single-layer solid target, which further reduces the influence of the Coulomb explosion field. Thus, the bunching field structure is maintained for the two-layer target and the proton bunch is drifting with a further energy gain, while the energy spread is reduced (see Fig. 3(d)), showing the obvious difference between the two-layer target and the single-layer solid target. Therefore, one observes that the proton bunch for the single-layer solid target expands in the longitudinal direction, while for the two-layer target the proton bunch is still compressed in a thin layer, as shown in Figs. 3(e) and 3(f). Finally, the proton bunch with peak energy of 192 MeV and energy spread of 12% is generated by the two-layer target, improving both the peak proton energy and the energy spread compared with the single-layer solid target (67 MeV with energy spread 57%). The divergence of the proton bunch for two-layer target and single-layer solid density target is 9° and 14°, respectively. The number of bunched protons (proton energy between 185 MeV and 195 MeV) for the two-layer target is about 3% of the total protons in the simulation box. Considering another dimension of 1 μm (which is about the focused laser spot size), this corresponds to a proton bunch number of the order of 10^7.

In order to check the robustness of this novel mechanism, the density and length of CDL plasma are scanned in the simulations. A total of 144 simulation results are run of CDL density from $0.1n_c$ to $10n_c$ and length from 1 μm to 100 μm, as shown in Fig. 4(a). It is observed that there exists an island of optimum parameter for CDL as shown in

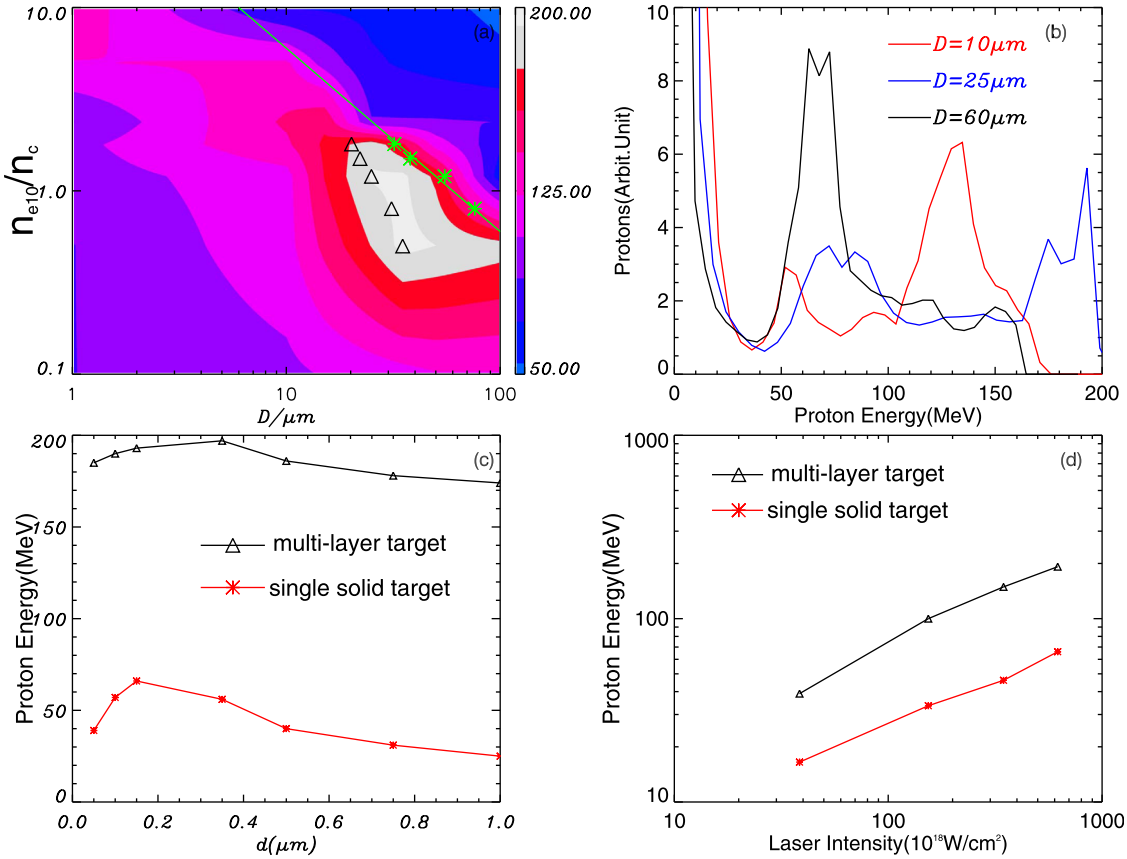

FIG. 4. Parameter scanning for CDL and proton energy scaling law. (a) The distribution of peak proton energy in plane of CDL plasma density n_{e10} and length D. The dark triangles and green stars denote the laser self-focusing length and depletion length in CDL in simulations. The green solid line shows the depletion length by the theoretical model by Eq. (1). (b) Proton energy spectrum at $t = 160T$ for CDL density of $1.2n_c$ and length of 10 μm, 25 μm, and 60 μm. (c) Peak proton energy for varied SDL thickness d. (d) Energy scaling for two-layer target with fixed near-critical plasma skin length $l_s/\lambda = \sqrt{an_c/n_{e10}} = 4.2$ and single-layer solid target.

Fig. 4(a). The optimal density is near the critical density (from 0.5 n_c to 2 n_c) and the optimal plasma length locates between the laser self-focusing length and the depletion length in the CDL. The laser depletion length can be estimated as[12]

$$D = 2c\tau_L n_c/n_{e10} = 60n_c/n_{e10}(\mu\text{m}), \qquad (1)$$

where τ_L is the laser duration. The proton energy spread of the high peak is smallest when the CDL length equals to the laser self-focusing length, as shown in Fig. 4(b), owing to the most efficient laser shaping process there.[18] For CDL thinner than optimal thickness, the laser self-focusing is less efficient and the energy conversion to DLA electrons is low. This results in a lower peak proton energy. For thicker CDL, the laser is almost completely depleted before it reaches SDL. In this case, as no laser interacts with the second SDL, the energy spectrum is flat in the high energy part (see in Fig. 4(b)). Fig. 4(c) shows that the peak proton energy is less sensitive to the thickness of SDL for the two-layer target than for the single-layer solid target, as the dominant electron acceleration happens in CDL. Fig. 4(d) implies that the proton energy for both targets scales as $E \propto I^{1/2}$. Here for the two-layer target, we keep the near-critical plasma skin length fixed to ensure the same laser shaping process for varied laser intensity.[18] It is shown that for the two-layer target the proton energy can be about three times higher than the single-layer solid target. We should note here that the self-focusing effect is less efficient in 2D case than 3D, which may make this mechanism even more efficient in 3D case.

In conclusion, we report a novel mechanism to realize efficient and stable proton acceleration with two-layer targets. It is shown by 2D PIC simulations that ~200 MeV proton beam with 12% energy spread can be generated with a realistic Gaussian LP laser pulse at laser intensity of 6×10^{20} W/cm^2, corresponding to about 0.9 PW laser power and 50 J laser energy. The proton energy is enhanced by a factor of 3 compared to single-layer solid targets due to the self-focusing and directly accelerated electrons in the critical density layer. Quasi-monoenergetic proton bunch is found for small proton/carbon ratio. The optimum acceleration is achieved when the length of CDL equals to the self-focusing length of the laser pulse. Such two-layer target can be realized by adding a foam layer onto a thin solid layer. In terms of the energy of the bunch and the energy spread, the proposed scheme seems to be promising for approaching ion beams parameters relevant to tumor therapy.

ACKNOWLEDGMENTS

This work was supported by National Natural Science Foundation of China (Grant Nos. 11025523, 10935002,

10835003, and J1103206) and National Basic Research Program of China (Grant No. 2011CB808104).

[1]M. Borghesi, D. H. Campbell, A. Schiavi, M. G. Haines, O. Willi, A. J. MacKinnon, P. Patel, L. A. Gizzi, M. Galimberti, R. J. Clarke, F. Pegoraro, H. Ruhl, and S. Bulanov, Phys. Plasmas **9**, 2214 (2002); S. V. Bulanova, T. Z. Esirkepov, V. S. Khoroshkov, A. V. Kuznetsov, and F. Pegoraro, Phys. Lett. A **299**, 240 (2002); M. Roth, T. E. Cowan, M. H. Key, S. P. Hatchett, C. Brown, W. Fountain, J. Johnson, D. M. Pennington, R. A. Snavely, S. C. Wilks, K. Yasuike, H. Ruhl, F. Pegoraro, S. V. Bulanov, E. M. Campbell, M. D. Perry, and H. Powell, Phys. Rev. Lett. **86**, 436 (2001); V. Malka, J. Faure, Y. A. Gauduel, E. Lefebvre, A. Rousse, and K. T. Phuoc, Nature Phys. **4**, 447 (2008); L. Robson, P. T. Simpson, R. J. Clarke, K. W. D. Ledingham, F. Lindau, O. Lundh, T. McCanny, P. Mora, D. Neely, C. G. Wahlström, M. Zepf, and P. McKenna, *ibid.* **3**, 58 (2007), and references therein.

[2]A. R. Smith, Med. Phys. **36**, 556 (2009); V. Malka, S. Fritzler, G. Grillon, J. Chambaret, A. Antonetti, D. Hulin, E. Lefebvre, E. d'Humieres, R. Ferrand, C. Albaret, and S. Meyroneinc, *ibid.* **31**, 1587 (2004).

[3]A. J. Mackinnon, Y. Sentoku, P. K. Patel, D. W. Price, S. Hatchett, M. H. Key, C. Andersen, R. Snavely, and R. R. Freeman, Phys. Rev. Lett. **88**, 215006 (2002); R. A. Snavely, M. H. Key, S. P. Hatchett, T. E. Cowan, M. Roth, T. W. Phillips, M. A. Stoyer, E. A. Henry, T. C. Sangster, M. S. Singh, S. C. Wilks, A. MacKinnon, A. Offenberger, D. M. Pennington, K. Yasuike, A. B. Langdon, B. F. Lasinski, J. Johnson, M. D. Perry, and E. M. Campbell, *ibid.* **85**, 2945 (2000); J. Fuchs, P. Antici, E. d'Humieres, E. Lefebvre, M. Borghesi, E. Brambrink, C. A. Cecchetti, M. Kaluza, V. Malka, M. Manclossi, S. Meyroneinc, P. Mora, J. Schreiber, T. Toncian, H. Pépin, and P. Audebert, Nature Phys. **2**, 48 (2005); J. Schreiber, F. Bell, F. Grüner, U. Schramm, M. Geissler, M. Schnürer, S. Ter-Avetisyan, B. M. Hegelich, J. Cobble, E. Brambrink, J. Fuchs, P. Audebert, and D. Habs, Phys. Rev. Lett. **97**, 045005 (2006).

[4]S. S. Bulanov, A. Brantov, V. Y. Bychenkov, V. Chvykov, G. Kalinchenko, T. Matsuoka, P. Rousseau, S. Reed, V. Yanovsky, K. Krushelnick, D. W. Litzenberg, and A. Maksimchuk, Med. Phys. **35**, 1770 (2008); B. Eliasson, C. S. Liu, X. Shao, R. Z. Sagdeev, and P. K. Shukla, New J. Phys. **11**, 073006 (2009); A. Macchi, S. Veghini, and F. Pegoraro, Phys. Rev. Lett. **103**, 085003 (2009); Z. M. Zhang, X. T. He, Z. M. Sheng, and M. Y. Yu, Phys. Plasmas **17**, 043110 (2010); A. Henig, S. Steinke, M. Schnürer, T. Sokollik, R. Hörlein, D. Kiefer, D. Jung, J. Schreiber, B. M. Hegelich, X. Q. Yan, J. Meyer-ter-Vehn, T. Tajima, P. V. Nickles, W. Sandner, and D. Habs, Phys. Rev. Lett. **103**, 045002 (2009); S. G. Rykovanov, J. Schreiber, J. Meyer-ter-Vehn, C. Bellei, A. Henig, H. C. Wu, and M. Geissler, New J. Phys. **10**, 113005 (2008); C. S. Liu, V. K. Tripathi, and X. Shao, AIP Conf. Proc. **1061**, 246 (2008); D. Jung, L. Yin, B. J. Albright, D. C. Gautier, R. Hörlein, D. Kiefer, A. Henig, R. Johnson, S. Letzring, S. Palaniyappan, R. Shah, T. Shimada, X. Q. Yan, K. J. Bowers, T. Tajima, J. C. Fernández, D. Habs, and B. M. Hegelich, Phys. Rev. Lett. **107**, 115002 (2011); X. Q. Yan, C. Lin, Z. M. Sheng, Z. Y. Guo, B. C. Liu, Y. R. Lu, J. X. Fang, and J. E. Chen, *ibid.* **100**, 135003 (2008).

[5]S. P. Hatchett, C. G. Brown, T. E. Cowan, E. A. Henry, J. Johnson, M. H. Key, J. A. Koch, A. B. Langdon, B. F. Lasinski, R. W. Lee, A. J. Mackinnon, D. M. Pennington, M. D. Perry, T. W. Phillips, M. Roth, T. C. Sangster, M. S. Singh, R. A. Snavely, M. A. Stoyer, S. C. Wilks, and K. Yasuike, Phys. Plasmas **7**, 2076 (2000).

[6]X. Q. Yan, H. C. Wu, Z. M. Sheng, J. E. Chen, and J. Meyer-ter-Vehn, Phys. Rev. Lett. **103**, 135001 (2009); M. Chen, A. Pukhov, T. P. Yu, and Z. M. Sheng, *ibid.* **103**, 024801 (2009).

[7]L. Yin, B. J. Albright, B. M. Hegelich, K. J. Bowers, K. A. Flippo T. J. T. Kwan, and J. C. Fernández, Phys. Plasmas **14**, 056706 (2007).

[8]H. B. Zhuo, Z. L. Chen, W. Yu, Z. M. Sheng, M. Y. Yu, Z. Jin, and R. Kodama, Phys. Rev. Lett. **105**, 065003 (2010).

[9]B. Qiao, S. Kar, M. Geissler, P. Gibbon, M. Zepf, and M. Borghesi, Phys. Rev. Lett. **108**, 115002 (2012).

[10]T. Esirkepov, M. Borghesi, S. V. Bulanov, G. Mourou, and T. Tajima, Phys. Rev. Lett. **92**, 175003 (2004).

[11]L. Willingale, S. P. D. Mangles, P. M. Nilson, R. J. Clarke, A. E. Dangor, M. C. Kaluza, S. Karsch, K. L. Lancaster, W. B. Mori, Z. Najmudin, J. Schreiber, A. G. R. Thomas, M. S. Wei, and K. Krushelnick, Phys. Rev. Lett. **96**, 245002 (2006); Y. Fukuda, A. Ya. Faenov, M. Tampo, T. A. Pikuz, T. Nakamura, M. Kando, Y. Hayashi, A. Yogo, H. Sakaki, T. Kameshima, A. S. Pirozhkov, K. Ogura, M. Mori, T. Zh. Esirkepov, J. Koga, A. S. Boldarev, V. A. Gasilov, A. I. Magunov, T. Yamauchi, R. Kodama, P. R. Bolton, Y. Kato, T. Tajima, H. Daido, and S. V. Bulanov, *ibid.* **103**, 165002 (2009).

[12]L. Willingale, S. R. Nagel, A. G. R. Thomas, C. Bellei, R. J. Clarke, A. E. Dangor, R. Heathcote, M. C. Kaluza, C. Kamperidis, S. Kneip, K. Krushelnick, N. Lopes, S. P. D. Mangles, W. Nazarov, P. M. Nilson, and Z. Najmudin, Phys. Rev. Lett. **102**, 125002 (2009).

[13]T. Nakamura, S. V. Bulanov, T. Z. Esirkepov, and M. Kando, Phys. Rev. Lett. **105**, 135002 (2010).

[14]A. V. Kuznetsov, T. Z. Esirkepov, F. F. Kamenets, and S. V. Bulanov, Plasma Phys. Rep. **27**, 211 (2001); K. Matsukado, T. Esirkepov, K. Kinoshita, H. Daido, T. Utsumi, Z. Li, A. Fukumi, Y. Hayashi, S. Orimo, M. Nishiuchi, S. V. Bulanov, T. Tajima, A. Noda, Y. Iwashita, T. Shirai, T. Takeuchi, S. Nakamura, A. Yamazaki, M. Ikegami, T. Mihara, A. Morita, M. Uesaka, K. Yoshii, T. Watanabe, T. Hosokai, A. Zhidkov, A. Ogata, Y. Wada, and T. Kubota, Phys. Rev. Lett. **91**, 215001 (2003); S. V. Bulanov and T. Z. Esirkepov, *ibid.* **98**, 049503 (2007); A. Yogo, H. Daido, S. V. Bulanov, K. Nemoto, Y. Oishi, T. Nayuki, T. Fujii, K. Ogura, S. Orimo, A. Sagisaka, J. L. Ma, T. Z. Esirkepov, M. Mori, M. Nishiuchi, A. S. Pirozhkov, S. Nakamura, A. Noda, H. Nagatomo, T. Kimura, and T. Tajima, Phys. Rev. E **77**, 016401 (2008); S. S. Bulanov, V. Yu. Bychenkov, V. Chvykov, G. Kalinchenko, D. W. Litzenberg, T. Matsuoka, A. G. R. Thomas, L. Willingale, V. Yanovsky, K. Krushelnick, and A. Maksimchuk, Phys. Plasmas **17**, 043105 (2010).

[15]A. Sgattoni, P. Londrillo, A. Macchi, and M. Passoni, Phys. Rev. E **85**, 036405 (2012).

[16]T. Nakamura, M. Tampo, R. Kodama, S. V. Bulanov, and M. Kando, Phys. Plasmas **17**, 113107 (2010).

[17]A. Pukhov and J. Meyer-ter-Vehn, Phys. Rev. Lett. **76**, 3975 (1996).

[18]H. Y. Wang, C. Lin, Z. M. Sheng, B. Liu, S. Zhao, Z. Y. Guo, Y. R. Lu, X. T. He, J. E. Chen, and X. Q. Yan, Phys. Rev. Lett. **107**, 265002 (2011).

[19]C. Gahn, G. D. Tsakiris, A. Pukhov, J. Meyer-ter-Vehn, G. Pretzler, P. Thirolf, D. Habs, and K. J. Witte, Phys. Rev. Lett. **83**, 4772 (1999); S. P. D. Mangles, B. R. Walton, M. Tzoufras, Z. Najmudin, R. J. Clarke, A. E. Dangor, R. G. Evans, S. Fritzler, A. Gopal, C. Hernandez-Gomez, W. B. Mori, W. Rozmus, M. Tatarakis, A. G. R. Thomas, F. S. Tsung, M. S. Wei, and K. Krushelnick, *ibid.* **94**, 245001 (2005).

[20]A. Pukhov, Z. M. Sheng, and J. Meyer-ter-Vehn, Phys. Plasmas **6**, 2847 (1999).

[21]M. Ashour-Abdalla, J. N. Leboeuf, T. Tajima, J. M. Dawson, and C. F. Kennel, Phys. Rev. A **23**, 1906 (1981); T. Tajima, D. Habs, and X. Q. Yan, Rev. Accel. Sci. Technol. **2**, 201 (2009).

[22]Z. M. Sheng, K. Mima, J. Zhang, and H. Sanuki, Phys. Rev. Lett. **94**, 095003 (2005).

[23]A. P. L. Robinson, A. R. Bell, and R. J. Kingham, Phys. Rev. Lett. **96**, 035005 (2006).